Progress in Oceanography 217 (2023) 103104

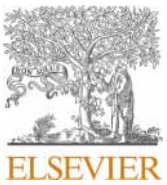

Contents lists available at ScienceDirect

Progress in Oceanography

journal homepage: www.elsevier.com/locate/pocean

Basin-scale variability in phytoplankton size-abundance spectra across the Atlantic Ocean

Cristina González-García [a,b], Susana Agustí [c], Jim Aiken [d], Arnaud Bertrand [e], Gabriel Bittencourt Farias [f], Antonio Bode [g], Claire Carré [e], Rafael Gonçalves-Araujo [h], Derek S. Harbour [d], María Huete-Ortega [a,b], Pedro A.M.C. Melo [f], Enrique Moreno-Ostos [i], Andrew P. Rees [d], Jaime Rodríguez [i], Sonia da Silva [j], Mikhail Zubkov [k], Emilio Marañón [a,b,*]

[a] Centro de Investigación Mariña da Universidade de Vigo (CIM-UVigo), Vigo, Spain
[b] Departamento de Ecología y Biología Animal, Universidade de Vigo, Vigo, Spain
[c] Red Sea Research Center, King Abdullah University of Science and Technology (KAUST), Saudi Arabia
[d] Plymouth Marine Laboratory, Plymouth, UK
[e] MARBEC, Université de Montpellier, CNRS, Ifremer, Institut de Recherche pour le Développement (IRD), Sète, France
[f] Departamento de Oceanografia, Universidade Federal de Pernambuco, Recife, Pernambuco, Brazil
[g] Instituto Español de Oceanografía (IEO-CSIC), Centro Oceanográfico de A Coruña, A Coruña, Spain
[h] National Institute for Aquatic Resources, Technical University of Denmark, Lyngby, Denmark
[i] Departmento de Ecología y Geología, Universidad de Málaga, Málaga, Spain
[j] Instituto Nacional de Investigação Pesqueira (INIP), Luanda, Angola
[k] Scottish Association for Marine Science, Oban, Argyll, UK

A B S T R A C T

Phytoplankton size structure, a major determinant of trophic structure and biogeochemical functioning in pelagic ecosystems, can be described by the slope of the size-abundance spectrum (SAS). Previous observational studies reporting spatio-temporal changes in phytoplankton SAS slope have focused on particular open-ocean or coastal environments. Therefore, the overall variability in phytoplankton SAS slope still has not been investigated over wide ranges of biomass and productivity including both oligotrophic open-ocean regions and productive coastal waters. Here we present a multi-cruise overview of the basin-scale variability in phytoplankton biomass and SAS slope across the Atlantic Ocean, covering coastal, shelf, and oceanic environments over the 50°N-50°S latitude range. We find the inverse relationship between cell size and abundance to be pervasive across the studied regions, even in highly productive coastal waters. In oceanic regions, consistent latitudinal patterns are observed in the relationship between nutricline depth, phytoplankton biomass and SAS slope. There is a strong degree of covariation between SAS slope at the surface and at the base of the euphotic layer, indicating that geographical changes in phytoplankton size structure override vertical variability. A basin-scale relationship exists between increasing resource supply, enhanced phytoplankton biomass, and progressively less steep SAS slopes, reflecting increasing importance of large cells in more productive waters. However, the relationship between ecosystem productivity and both SAS slope and mean community cell size is saturating, which means there is no continuous trend towards ever increasing contribution by larger cells. Similar phytoplankton size structures, with a biomass dominance by the 2–20 μm size class, are found in both moderately and highly eutrophic waters. Our results provide an observational benchmark for testing the predictions of size-based plankton models and for assessing future, climate-related shifts in phytoplankton size structure in both coastal and oceanic regions of the Atlantic Ocean.

1. Introduction

Phytoplankton size structure is a major determinant of trophic structure and biogeochemical functioning in pelagic ecosystems, affecting the length and complexity of the food web, energy transfer efficiency, the fate of primary production, and the strength of the biological carbon pump (Marañón, 2015; Sommer et al., 2017, Hillebrand et al., 2022). Communities dominated by small cells, such as those of nutrient-impoverished regions, support complex food webs with a high recycling efficiency that have a small potential for atmospheric CO_2 drawdown and organic carbon export. In contrast, a dominance by larger species, which is typical of nutrient-rich, productive waters, is associated with simpler trophic pathways, enhanced sinking rates, and larger fractions of exported primary production. The variability in phytoplankton size structure is thus a fundamental component of the biogeography of plankton functional traits (Barton et al., 2013).

* Corresponding author at: Centro de Investigación Mariña da Universidade de Vigo (CIM-UVigo), Vigo, Spain.
E-mail address: em@uvigo.es (E. Marañón).

https://doi.org/10.1016/j.pocean.2023.103104
Received 20 March 2023; Received in revised form 14 July 2023; Accepted 4 August 2023
Available online 5 August 2023

A commonly used approach to characterize the size distribution of species assemblages in aquatic ecosystems is to construct an individual size distribution, also known as size-abundance spectrum (SAS) (White et al., 2007). In a SAS, all size classes have the same width on a logarithmic scale and the total abundance (N) of all individuals, irrespective of species, within each size class is plotted as a function of the nominal cell size of the size class (Rodríguez et al., 1998; Rodríguez et al., 2002). The resulting abundance distribution follows a decreasing power function of cell volume (V) such that $N \propto V^b$, where b, the size scaling exponent, typically takes a negative value. Logarithmic transformation gives $\log N = a + b \log V$, where a and b are the intercept and slope, respectively, of the log-transformed relationship. The slope of the SAS is a general indicator of the relative importance of cells of different size in terms of their contribution to total biomass.

Previous studies have described the variability in SAS slopes from specific cruises or research programs focused on particular oceanic or coastal environments. Slope values are usually between −1.3 and −0.9 in low-latitude, open-ocean regions (Cavender-Bares et al., 2001; Huete-Ortega et al., 2012; Moreno-Ostos et al., 2015), where small cells contribute most of the biomass, and between −0.9 and −0.6 in coastal waters dominated by larger cells (Reul et al., 2005; Marañón et al., 2007; Huete-Ortega et al., 2010). These results support a linkage between nutrient availability and the steepness of the SAS, such that slopes become less negative as nutrient supply increases. This pattern arises from the competitive advantage of small cells with high nutrient affinity in oligotrophic environments (Raven, 1998), the superior ability of larger cells to convert nutrients into biomass and sustain fast growth rates under nutrient-rich conditions (Marañón, 2015, Hillebrand et al., 2022), and the fact that mortality losses due to grazing decrease with increasing cell size (Armstrong, 1994, Ward et al., 2012, Pančić and Kiørboe, 2018). However, the relationship between resource supply and phytoplankton size-abundance distribution still has not been quantified across wide trophic gradients ranging from open-ocean oligotrophic to coastal highly productive waters.

Size-fractionated chlorophyll *a* data (Raimbault et al., 1988; Marañón et al., 2001, 2012) and the results of size-based ecological models (Armstrong, 1994; Poulin and Franks, 2010; Ward et al., 2014) suggest that, as total phytoplankton biomass increases, the biomass in each size class grows until it reaches an upper limit, which is higher for progressively larger cell sizes. This means that, across wide ranges of variability, phytoplankton biomass can increase only if larger size classes are added, which would lead to a continuous increase in the contribution of large cells as standing stocks grow (Chisholm, 1992). We should thus expect the slope of the SAS to become less and less negative as total phytoplankton biomass keeps increasing. This prediction, however, has not yet been examined due to a lack of studies addressing the variability of SAS slopes over sufficiently broad ranges of biomass and productivity, including open-ocean oligotrophic regions as well as productive continental-shelf and coastal waters.

Here we present a multi-cruise overview of the basin-scale variability in the slope of phytoplankton size-abundance (SAS) spectra in the Atlantic Ocean covering coastal, shelf, and open-ocean environments over the 50°N-50°S latitudinal range. The analysis is based on a dataset of > 700 phytoplankton samples collected during > 30 cruises over a 27-year period. Our aim is to identify general patterns in the large-scale geographical variability of phytoplankton biomass and SAS slopes, provide an observational benchmark for size-based plankton models, and gain insight into the mechanisms and drivers underlying changes in phytoplankton size structure across a wide productivity range.

2. Materials and methods

2.1. Data collection

Phytoplankton abundance and cell size, together with complementary oceanographic variables, were measured during > 30 oceanographic cruises conducted within the period 1995–2022 in coastal and open-sea waters of the Atlantic Ocean, including the central, subtropical and tropical Atlantic, the Equatorial region, the continental shelf from Mar del Plata to South Brazil, the Angola continental shelf, the Benguela upwelling region, and the coastal upwelling region of the NW Iberian Peninsula (Table S1, Fig. S1). The resulting dataset contains phytoplankton abundance and size data for a total of 706 samples.

2.2. Hydrography, nutrients and chlorophyll a

Vertical profiles of temperature and salinity were obtained in all cruises with a Conductivity-Temperature-Depth (CTD) probe. Samples for the determination of phytoplankton abundance and, in some cruises, additional variables such as inorganic nutrient and chlorophyll *a* concentration were collected with Niskin bottles from multiple depths in the euphotic layer. Vertical profiles of photosynthetically active radiation (PAR) were obtained during cruises AMT1-3 and during the NW Iberian Peninsula costal survey, using a SeaOPS Satlantic sensor and a LI-193LI-COR sensor, respectively (Marañón et al., 2004, 2000). For other cruises, and only at open-ocean locations, the depth of the euphotic layer (1 % PAR_z) was estimated from the depth of the deep chlorophyll maximum (DCM_z) using the empirical equation obtained by Huete-Ortega et al. (2011) in the tropical Atlantic: $1\ \%PAR_z = 9.3 + 0.98 \times DCM_z$.

Nitrate concentration was determined using segmented-flow automatic analyser techniques (Gonçalves-Araujo et al., 2018, 2012; Marañón et al., 2004, 2000). For cruises AMT1-4, Trynitrop 1 and Malaspina, nitrate concentration was determined at > 10 depths over the 0–200 m range. The nitracline depth, a proxy for nutrient supply into the euphotic layer (Cermeño et al., 2008), was defined as the first depth at which nitrate concentration was > 1 μmol/L. Total chlorophyll *a* concentration throughout the euphotic layer was measured by HPLC, after filtration onto glass-fibre Whatman GF/F filters (Gonçalves-Araujo et al., 2018, 2012), or by fluorometry after filtration through 0.2-μm polycarbonate filters and extraction in 90% acetone (Huete-Ortega et al., 2011; Marañón et al., 2004, 2001).

For stations with nutrient profiles, we calculated the resource supply index (RSI) (Marañón et al., 2014), which takes into account the concentration of nitrate at the bottom of the euphotic layer ($NO_3^-[1\%PAR]$), the density difference between the surface and the base of the euphotic layer ($\Delta\sigma_t$), the depth of the euphotic layer ($1\%PAR_z$), and the depth of the upper mixed layer (UML_z), defined as the first depth at which σ_t is 0.125 units higher than the surface value:

$$RSI = \frac{NO_3^-[1\%PAR]}{\Delta\sigma t} \times \frac{1\%PARz}{UMLz}$$

The first term in the RSI formula represents nutrient supply, which is expected to increase with nitrate concentration at the base of the euphotic layer but decreases as vertical stratification intensifies, which results in larger seawater density differences between the surface and the base of the euphotic layer. The second term discriminates conditions in which cells are confined within a shallow upper mixed layer, relative to the depth of the euphotic layer, and thus are exposed to high irradiances on average, from conditions in which the depth of the upper mixed layer equals or exceeds the penetration of irradiance into the water column, therefore leading to light limitation of phytoplankton growth.

2.3. Phytoplankton size-abundance spectra

The abundance and cell volume of picophytoplankton (<2 μm in cell diameter) and small nanophytoplankton (2–5 μm) were measured by flow cytometry from fixed samples during cruises AMT3-4 (Zubkov et al., 1998; Zubkov and Sleigh, 2000), Trynitrop 1 (Huete-Ortega et al., 2011) and Abraços 2 and from fresh samples during Malaspina (Moreno-Ostos et al., 2015). The abundance and cell volume of larger cells, from large nanophytoplankton (5–20 μm) to microphytoplankton (>20 μm), were determined in all cruises by microscopy, using 50–100 mL samples preserved in 1% Lugol's iodine solution and following the Utermöhl method.

For Trynitrop 1 and Malaspina cruises and for the NW Iberia embayment survey, cell biovolumes were calculated using specific image analysis software to determine the shape, length, and width of each cell present in the sample (Huete-Ortega et al., 2011; Marañón et al., 2004; Moreno-Ostos et al., 2015). This method resulted in the ataxonomic determination of cell abundance and biovolume. During Trynitrop 1 and Malaspina cruises, larger cells (>5 μm for Trynitrop 1 and > 20 μm for Malaspina) were counted from larger-volume samples (2–5 L) concentrated by gravity filtration through 5-μm polycarbonate filters or a 15-μm nylon mesh (Huete-Ortega et al., 2011, Moreno-Ostos et al., 2015). For cruises AMT1-4, Abraços 2, Meteor M48/5, ACEx, and PATEX, samples were processed according to the Utermöhl method, typically using samples of 50–100 mL in volume. In the case of Abraços 2, larger cells were counted from larger-volume samples concentrated by gravity filtration as explained above. Cells were counted and identified to species or nearest taxonomic level and their biovolume was determined based on the geometric shape and dimensions of each classified organism (Gonçalves-Araujo et al., 2018, 2012; Sal et al., 2013). A specific cell volume value was assigned to each phytoplankton species, resulting in a taxonomic assessment of phytoplankton cell abundance and biovolume. When biovolume measurements were not available for the identified species, cell volumes were assigned based on the data given by Sal et al. (2013) and other databases of phytoplankton species biovolume (Harrison et al., 2015, Karlson et al., 2020; Olenina et al., 2006).

Phytoplankton size-abundance spectra (SAS) were constructed by calculating the total cell abundance in each of 26 size classes, covering the size range from the smallest picophytoplankton (0.5 μm in equivalent spherical diameter, ESD) to the largest observed microphytoplankton (160 μm ESD). Size classes were defined according to an octave ($\log_2$) scale of cell volume, where size class width equals the value of the size class lower limit and nominal volume. Each SAS was obtained by plotting $\log_{10}$-transformed total cell abundance (*y*-axis, cell mL^{-1}) as a function of $\log_{10}$-transformed cell volume for each size class (*x*-axis, μm^3). Linear regression was used to obtain the slope and intercept of the relationship between log cell size and log abundance. Of all SAS constructed ($n = 706$), 31% had r^2 values > 0.9, 38% had r^2 values between 0.7 and 0.9, 14% had r^2 values between 0.5 and 0.7, and 17% had r^2 values < 0.5.

We assessed the extent to which the taxonomic (traditional microscopy) versus ataxonomic (image analysis) assessment of large nano- and microphytoplankton yield consistent results, by comparing SAS obtained with both methods in the same open-ocean region (from 10°N to 30°S) during different cruises. SAS obtained with the ataxonomic approach extended to larger size classes, because the larger sample volume allowed better detection of rare, large (>10,000 μm^3) cells. However, the two methods resulted in similar slope and intercept values (Fig. S2), which supports their combined use to depict broad-scale patterns of variability in phytoplankton size structure.

Total phytoplankton carbon biomass was calculated by multiplying the cell abundance in each size class by its cell biomass, and then adding together the resulting biomass of all size classes. For the nano- and microphytoplankton, cell volume (*V*, μm^3 cell^{-1}) was converted into carbon biomass (*C*, pgC cell^{-1}) using the carbon-volume relationship obtained by Marañón et al. (2013) ($C = 0.21\ V^{0.88}$). For the picophytoplankton, cell abundance was converted into biomass by applying the conversion factors given by Buitenhuis et al. (2012) (0.060 pgC cell^{-1} for *Prochlorococcus*, 0.154 pgC cell^{-1} for *Synechococcus*, and 1.32 pgC cell^{-1} for picoeukaryotes).

3. Results

3.1. Variability in phytoplankton SAS slope across the Atlantic Ocean

The inverse relationship between phytoplankton cell size and abundance was pervasive across the different cruises and surveys, as indicated by the fact that 70% of all SAS had determination coefficients (r^2) above 0.7. Phytoplankton SAS with a strong degree of linearity (i.e., with $r^2 \geq 0.7$) were obtained from samples in which the entire cell size range had been examined (Fig. 1a-c,f) but also from those in which only

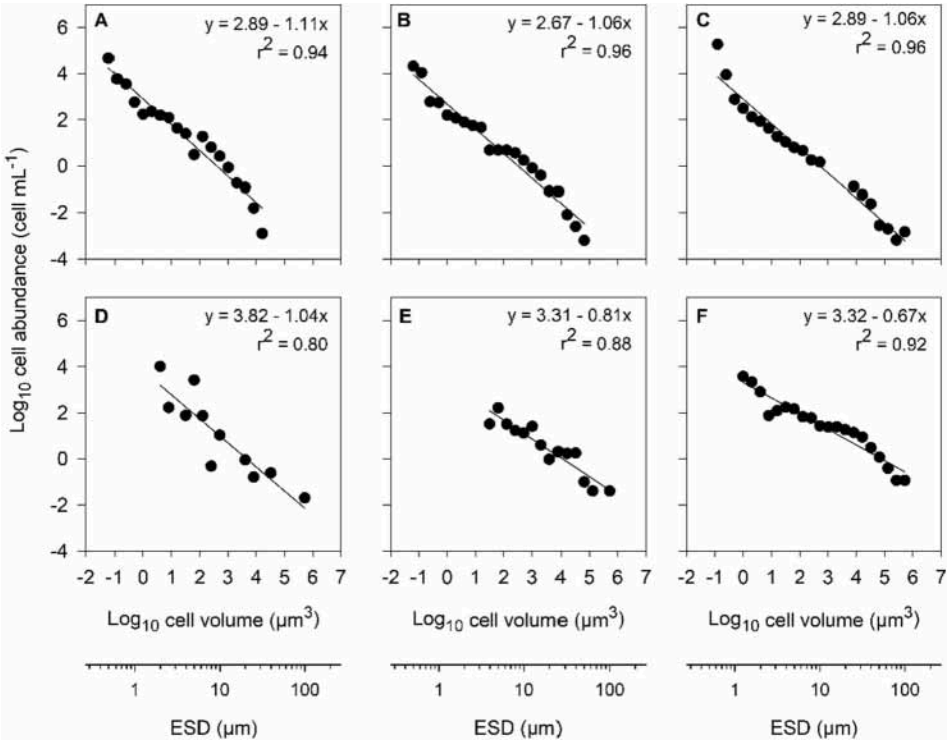

Fig. 1. Examples of phytoplankton size-abundance spectra from six locations in coastal and oceanic regions of the Atlantic Ocean: (A) subtropical North Atlantic (cruise Trynitrop 1), (B) subtropical South Atlantic (Trynitrop 1), (C) Equator (Malaspina), (D) Benguela upwelling (Meteor M48/5), (E) South Brazil continental shelf (ACEx) and (F) Ría de Vigo (NW Iberian peninsula). The *x*-axis at the bottom indicates the equivalent spherical diameter (ESD).

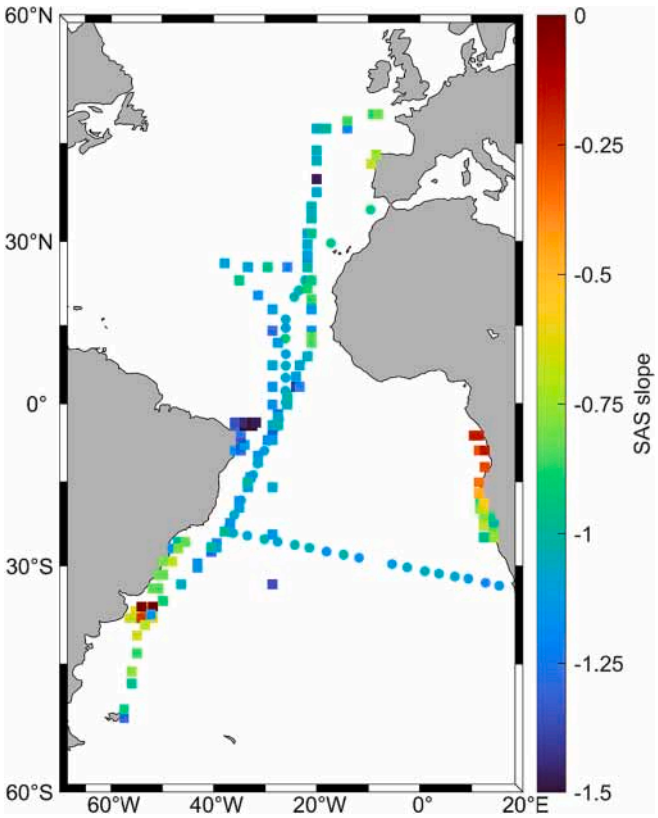

Fig. 2. Geographical variability in the slope of the phytoplankton size-abundance spectrum (SAS) across the Atlantic Ocean. The available estimates of phytoplankton SAS slope were averaged over each 1°×1° grid. Surface SAS slopes are represented by a square and include data from cruises AMT1-4, Trynitrop 1, Abraços 2, ACEx, PATEX, Meteor M48/5, Angola monitoring lines, annual surveys of Ría de Vigo (NW Iberian peninsula) and a coastal time series off A Coruña (NW Iberian peninsula). Data from Malaspina cruise, indicated by circles, correspond to samples obtained at the DCM.

nano- and microphytoplakton cells had been counted (Fig. 1d,e). In open-ocean locations, slope values typically ranged between −0.6 and −1.2, with a general tendency for steeper (more negative) slopes in tropical and subtropical regions and shallower (less negative) slopes in temperate latitudes (Fig. 2). Samples with very shallow SAS (slopes between −0.2 and −0.4) were found only in shelf waters off Angola and in some stations of the north Patagonian shelf-break. We summarize below the observed patterns of variability in hydrography and phytoplankton biomass and size structure, first considering changes in mean values over 10° latitudinal bands as ascertained from open-ocean cruises along the central Atlantic, and then by comparing the main coastal and oceanic regions sampled.

3.2. Hydrography, phytoplankton biomass, and size structure along 50°N–50°S

Mean sea surface temperature ranged from ca. 15 °C at 40–50°N and ca. 10 °C at 40–50°S to 27–28 °C in the Equatorial region (10°N–10°S), with wider variability at temperate latitudes reflecting stronger seasonality (Fig. 3a). The depth of the nutricline also described marked latitudinal patterns (Fig. 3b). The deepest nutriclines (>150 m) were observed in the south subtropical gyre (10–30°S), whereas the shallowest ones (<70 m) were recorded in temperate latitudes (40–50°N and 40–50°S) and also between 10 and 20°N, corresponding to the Mauritanian upwelling region. The patterns of latitudinal variability in both surface chlorophyll *a* concentration (Chl *a*) (Fig. 3c) and surface phytoplankton biomass (Fig. 3d) were opposite to those of the nutricline

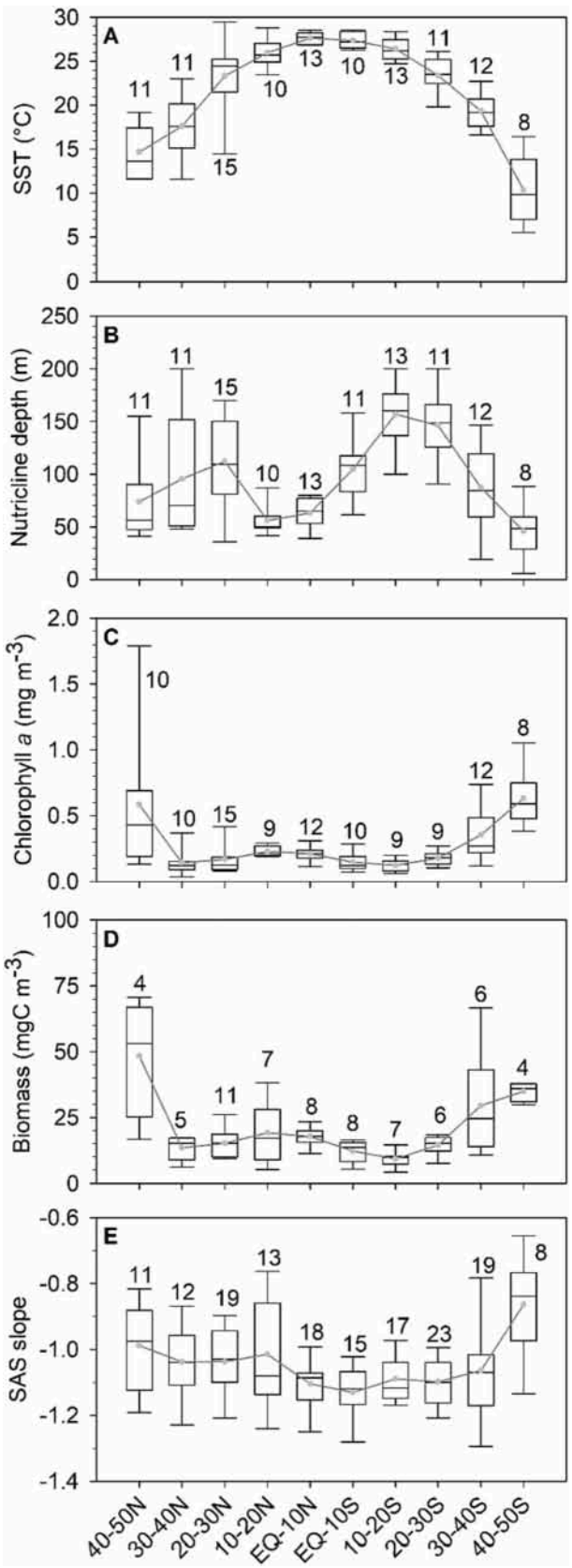

(caption on next page)

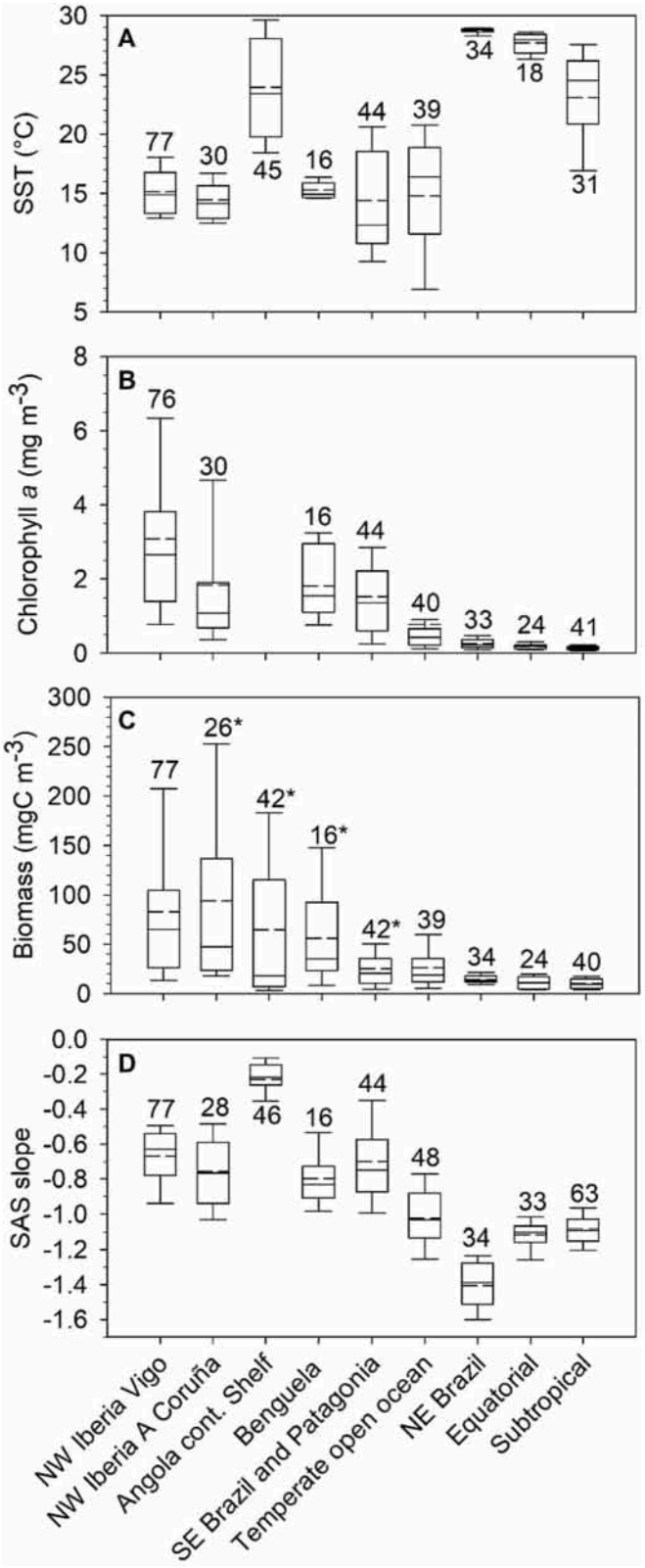

Fig. 3. Latitudinal variability of (A) sea surface temperature (°C), (B) nutricline depth, (C) surface chlorophyll *a* concentration (mg m^{-3}), (D) surface phytoplankton biomass (mg C m^{-3}) and (E) slope of the phytoplankton size-abundance spectrum from 50°N to 50°S in the Atlantic Ocean. The grey line and small circles represent the mean. Solid lines indicate the median, boxes encompass the 25% and 75% percentiles, and whiskers encompass the 10% and 90% percentiles. The number of observations for each variable and latitudinal band is given on top of each box. Original data were obtained from cruises AMT1-4, Trynitrop and Malaspina, except for panel D, which includes data from AMT3-4 and Trynitrop 1 only.

depth. The lowest mean Chl *a* values (around 0.1 mg m^{-3}) were measured in the subtropical gyres, coinciding with the deepest nutriclines, whereas higher Chl *a* was observed in the Equatorial region (0.2–0.3 mg m^{-3}) and in temperate latitudes (>0.5 mg m^{-3}), in both cases associated with shallower nutriclines. Similarly, surface phytoplankton biomass took mean values around 10–15 mgC m^{-3} at the subtropical gyres, increasing to > 15 mgC m^{-3} in the regions affected by the equatorial upwelling and the Mauritanian coastal upwelling and to > 30 mgC m^{-3} in temperate latitudes (Fig. 3d). Using the mean values for 10°-latitudinal bands, significant inverse relationships were identified between nutricline depth and both Chl *a* (Fig. S3a) and phytoplankton biomass (Fig. S3b).

The slope of the phytoplankton SAS typically ranged between −0.8 and −1.2 across 50°N–50°S (Fig. 3e). The steepest mean slopes (around −1.1), indicating a marked dominance by small cells, were observed between 10°N and 30°S, whereas less steep slopes (between −0.8 and −1.0), corresponding to enhanced contribution by larger cells, were found in temperate latitudes and between 10 and 20°N. The latter latitudinal band exhibited a wide range of SAS slopes, reflecting the fact that some cruises sampled the Mauritanian upwelling region along 20°W, characterized by increased phytoplankton biomass and shallower slopes, whereas others took place in more oligotrophic waters along 30°W and further west (Fig. S1). There was a significant inverse relationship between nutricline depth and SAS slope, such that shallower nutriclines were associated with less steep slopes (Fig. S3c). Both Chl *a* (Fig. S3d) and phytoplankton biomass (Fig. S3e) were positively correlated with SAS slope, as regions with larger phytoplankton standing stocks tended to show less steep slopes.

3.3. Region-specific variability in phytoplankton biomass and size structure

The comparison of mean values and ranges of variability from coastal and shelf waters to oceanic regions describes a broad trend of decreasing Chl *a* and biomass together with a steepening of SAS slopes (Fig. 4). In the most productive sites sampled, located in the coastal upwelling region off NW Iberia, the highest levels of phytoplakton biomass reached 200–250 mgC m^{-3} and mean values were around 90 mgC m^{-3} (Fig. 4c), while SAS slopes typically ranged between −0.7 and −0.9 (Fig. 4d). In the opposite end of the productivity gradient, tropical and equatorial open-ocean waters had mean biomass levels < 10 mgC m^{-3} and SAS slopes around −1.1. Temperate open-ocean regions had intermediate values of biomass (ca. 30 mgC m^{-3}) and SAS slope (ca. −1.0) (Fig. 4d), while more extreme mean SAS slopes were recorded in the Angolan shelf (ca. −0.2) and in oceanic waters off NE Brazil (ca. −1.4).

3.4. Vertical variability in SAS slope

We assessed the changes in phytoplankton size structure over depth by comparing the SAS slope in surface waters and at the depth of the deep chlorophyll maximum (DCM) (Fig. 5). Surface and DCM slopes strongly covaried (Pearson's $r = 0.68$, $p < 0.0001$, $n = 92$), indicating that large-scale geographical variability largely overrides depth-related

(caption on next page)

Fig. 4. Variability of (A) sea surface temperature (°C), (B) surface chlorophyll *a* concentration (mg m^{-3}), (C) surface phytoplankton biomass (mg C m^{-3}) and (D) slope of the phytoplankton size-abundance spectrum in nine coastal and oceanic regions of the Atlantic Ocean. Original data were obtained during cruises AMT1-4, Trynitrop 1, Malaspina, Abraços 2, ACEx, PATEX, Meteor M48/5, Angola's INIP time series, two annual surveys of Ría de Vigo (NW Iberian peninsula) and a coastal time series off A Coruña (NW Iberian peninsula). Data from open-ocean latitudinal cruises (AMT1-4, Trynitrop 1 and Malaspina) are divided into temperate (30–50°N, 30–50°S), equatorial (10°N–10°S) and subtropical regions (10–30°N, 10–30°S). Data from AMT stations located near the Mauritanian upwelling region (10–25°N along 20°W) are not included here. Chlorophyll *a* concentration data were not available for the Angola monitoring lines. In (C), an asterisk indicates that the estimate of phytoplankton biomass does not include the picophytoplankton.

variability in phytoplankton size structure. Although in most cruises the vertical sampling resolution was coarse, with at most 2–3 samples being collected at each site, during the AMT3 cruise additional samples were taken at some locations, including two strongly stratified stations in the equatorial and south subtropical Atlantic (Fig. S4). At both sites a DCM was present, with the increase in Chl *a* (relative to the surface value) in the equatorial station being twice as large as that of the subtropical station (Fig. S4a,b). The DCM represented a moderate biomass maximum in the equatorial site but not in the subtropical site, where phytoplankton biomass was invariant over depth (Fig. S4c,d). In both stations the slope of the SAS showed little variation with depth, indicating similar phytoplankton size structure throughout the euphotic layer (Fig. S4e,f).

3.5. Changes in SAS slope along a wide productivity gradient

The overall pattern in the relationship between ecosystem productivity and phytoplankton size structure can be ascertained by plotting SAS slope and mean cell diameter as a function of surface Chl *a* (Fig. 6), which has been shown to be a good predictor of surface primary production over broad ranges of variability (Marañón et al. 2014, their Fig. 1b). The relationships shown in Fig. 6 were best fitted by a non-linear, saturating model, which was superior to the linear model as it yielded lower values of the Akaike Information Criterion and also explained a larger amount of variance in SAS slopes. Although the variability in oligotrophic waters is large, as Chl *a* increases from < 0.1 to ca. 1 mg m^{-3} there is a tendency for slopes to become less negative, indicating a growing contribution of larger cells (Fig. 6a). This trend, however, does not continue for Chl *a* levels above 1 mg m^{-3}, because similar SAS slopes values (between −0.9 and −0.7) are found in samples with moderately high (1–2 mg m^{-3}) and very high Chl *a* (>4 mg m^{-3}). We also plotted SAS slopes as a function of log-transformed Chl *a* for samples with Chl *a* below and above 2 mg m^{-3} (Fig. S5) and found a marked change in the slope of the relationship from one group of samples to the other. The trend towards less steep SAS slopes with increasing Chl *a*, which is observed in low-Chl *a* samples (Fig. S5a), virtually disappears in high-Chl *a* samples (Fig. S5b). The saturating relationship between phytoplankton standing stocks and size structure is also observed when mean cell diameter (computed as the biomass-weighted geometric mean of ESD) is plotted as a function of Chl *a* (Fig. 6b). Mean cell diameter becomes larger as Chl *a* increases until approximately 2 mg m^{-3} but then stabilizes, suggesting that both mesotrophic and eutrophic environments have similar phytoplankton size structure.

We used data from Ría de Vigo, which is the only coastal, highly productive ecosystem in which cell abundance had been measured across the entire cell size range, to calculate the biomass contribution by picophytoplankton (cells < 2 μm in cell diameter), nanophytoplankton (2–20 μm) and microphytoplankton (>20 μm) in surface samples during conditions of moderately high and very high phytoplankton abundance (Fig. S6). The partitioning of biomass among the three size classes was similar in samples with moderately high (1–2 mg m^{-3}) and very high Chl *a* (>4 mg m^{-3}). While the picophytoplankton biomass share was larger in samples with moderately high Chl *a* than in samples with very high Chl *a*, nanophytoplankton was the dominant size class (>50% of total biomass) in both groups of samples.

The potential effect of temperature on phytoplankton size structure was assessed by plotting the SAS slope as a function of sea surface temperature (SST) for samples collected in open-ocean and coastal regions (Fig. S7). We found no significant relationship between the two variables, and SST explained a negligible amount of the variability in SAS slope ($r^2 = 0.01$).

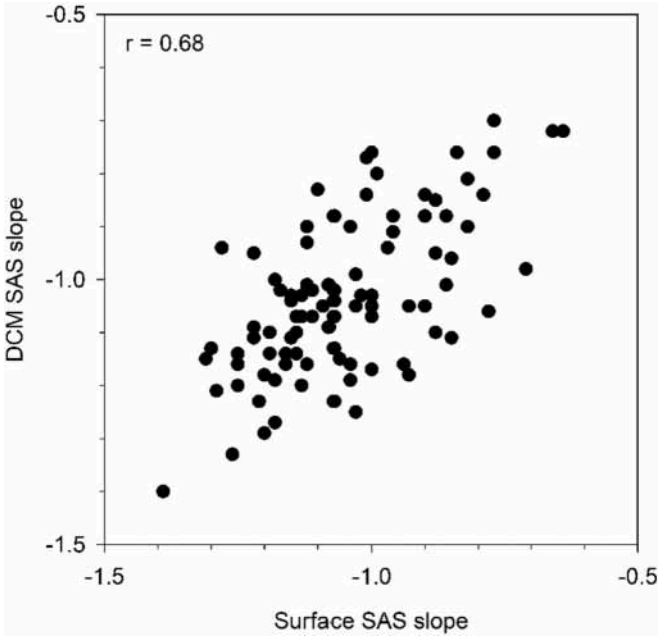

Fig. 5. Relationship between the slope of the phytoplankton size-abundance spectrum determined in surface versus DCM samples across the Atlantic Ocean during cruises AMT1-4 and Trynitrop 1. The correlation between surface and DCM slopes was highly significant (Pearson's $r = 0.68$, $p < 0.0001$, $n = 92$).

3.6. Relationship between resource supply and phytoplankton biomass and SAS slope

We calculated the resource supply index (RSI) in different open-ocean and coastal regions of the Atlantic Ocean and investigated its relationship with phytoplankton standing stocks (represented by Chl *a* and carbon biomass) and phytoplankton size structure (represented by the SAS slope) (Fig. 7). Due to the large geographical differences in both nutrient concentration at the base of the euphotic layer and the magnitude of the vertical density gradient, most of the variability in RSI was due to changes in nutrient availability. Linear regression analysis indicated that the nutrient term and the irradiance term explained 40% and 10%, respectively, of the variability in RSI.

The progressive increase in RSI from the oceanic subtropical regions to the temperate oceanic regions and finally the coastal ecosystems drives an increase in both Chl *a* and phytoplankton biomass (Fig. 7a,b). However, the increase in mean Chl *a* from the most oligotrophic to the most productive ecosystems (ca. 30-fold) is larger than that observed in terms of mean phytoplankton carbon (ca. 10-fold), suggesting a decrease of the C:Chl *a* ratio as trophic status increases. This pattern is more clearly visible in the relationship between phytoplankton carbon and Chl *a* ratio using the original, unaggregated data (Fig. S8). There is a strong covariation between the estimated phytoplankton carbon and the measured Chl *a*, but the slope of the relationship is significantly higher than 1 (1.49), indicating that as we move from oligotrophic to eutrophic waters Chl *a* increases much faster than phytoplankton biomass does.

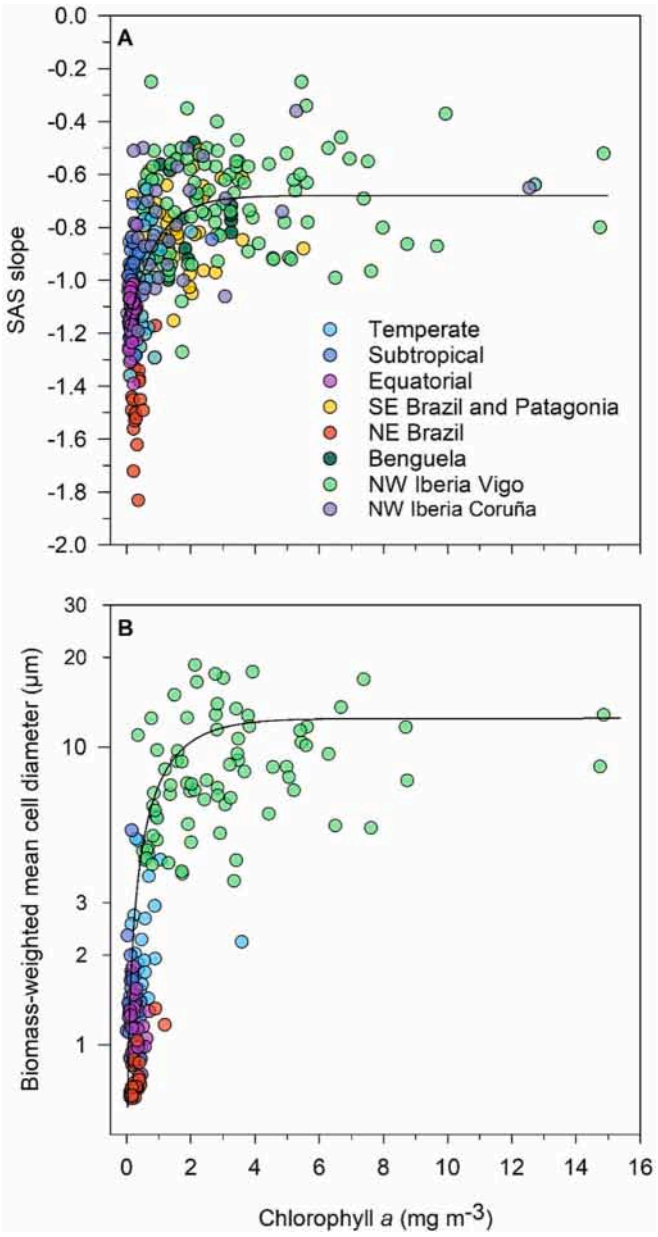

Fig. 6. Relationship between surface chlorophyll *a* concentration and (A) the slope of the size-abundance spectrum and (B) mean cell diameter (ESD) for the entire phytoplankton assemblage. Mean ESD was calculated as the biomass-weighted geometric mean. The non-linear fits are (a) $y = -1.21 + 0.53\ (1\text{-}e^{-1.19x})$ ($r^2 = 0.45$, $p < 0.0001$, $n = 366$) and (b) $y = 0.30 + 12.18\ (1\text{-}e^{-0.65x})$ ($r^2 = 0.43$, $p < 0.0001$, $n = 203$). Data in (a) were obtained from cruises AMT1-4, Abraços 2, ACEx, PATEX, Meteor M48/5, Trynitrop, annual surveys of Ría de Vigo (NW Iberian peninsula) and a coastal time series off A Coruña (NW Iberian Peninsula). In (b), biomass-weighted mean cell diameter was calculated only for surface samples in which phytoplankton abundance had been determined across the entire cell size range, namely cruises AMT3-4, Trynitrop 1, Abraços 2 and the annual surveys of Ría de Vigo.

Finally, the biogeographic trend of increasing resource supply and phytoplankton biomass is associated with a shallowing of the mean SAS slope, from ca. −1.1 in tropical and equatorial regions to values closer to −1.0 in oceanic temperate regions and near −0.8 in coastal, highly productive ecosystems (Fig. 7c).

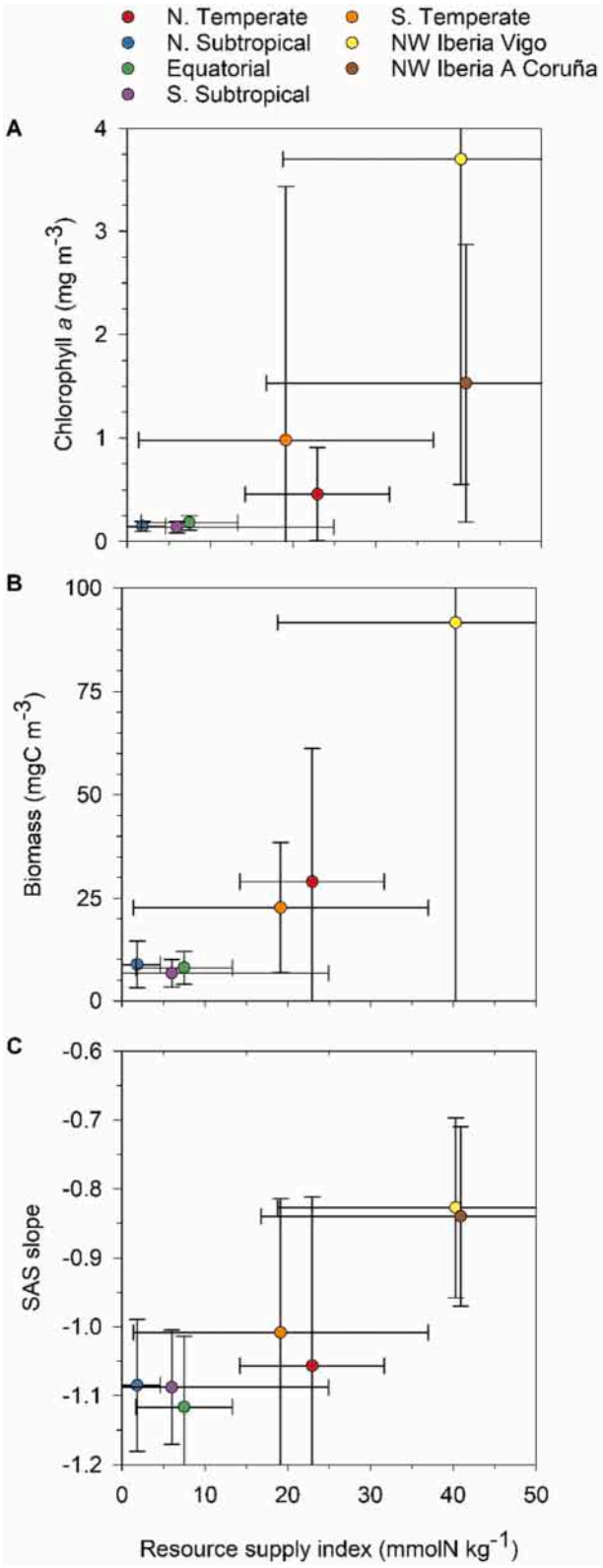

Fig. 7. Relationship between resource supply index (RSI) and (A) chlorophyll *a* concentration, (B) phytoplankton biomass and (C) slope of the size abundance spectrum in surface samples from different regions of the Atlantic Ocean. For each region, mean values and their standard deviations are plotted. Open-ocean data were obtained from cruises AMT3-4 and Trynitrop 1, while coastal data correspond to the annual survey of Ría de Vigo (NW Iberian peninsula) conducted in 2001–2002 and a coastal time series off A Coruña (NW Iberian peninsula). See Methods for details on the calculation of RSI.

4. Discussion

Our analysis combines measurements from > 700 phytoplankton samples obtained in ca. 30 coastal and open-ocean cruises and surveys over a period of 27 years. In spite of methodological differences among cruises, we have identified coherent patterns of cross-system variability in phytoplankton size-abundance spectra (SAS), including i) strong covariation between SAS slopes at the surface and the base of the euphotic layer, ii) linkage between resource supply and mean slope across biogeographic regions, and iii) asymptotic relationship between phytoplankton standing stock and size structure as represented by SAS slope and mean community cell size.

4.1. Methodological considerations

The above conclusions are robust against uncertainties introduced by combining microscopy measurements of phytoplankton cell size and abundance obtained from multiple operators. While sample volume and preservation, as well as settling procedure, were broadly consistent among studies, there might have been differences in the detection of cells (particularly in the case of small nanophytoplankton) and the estimation of cell biovolumes. When assigned difficult identification tasks, expert phytoplankton taxonomists can attain accuracies of 84–95%, while trained personnel achieve 67–83% self-consistency and 43% consensus (Culverhouse et al., 2003). For the purposes of our analysis, however, the correct taxonomic labelling is less critical than the correct assignation of each counted cell to its appropriate size class. The assumption of constant cell volume for each species in the case of samples subjected to taxonomic analysis may have also introduced error, because the same species can change in size depending on growth conditions (Peter and Sommer, 2013; Orizar and Lewandowska, 2022). Nevertheless, spatial and temporal changes in overall phytoplankton size structure (e.g. SAS slope, partitioning of biomass among size classes) are overwhelmingy dominated by changes in species composition rather than by changes in intrapopulation mean cell size (Marañón et al., 2012, Sommer et al., 2017). The remarkable agreement between the mean SAS slope observed in the central tropical and subtropical Atlantic (10°N–30°S) from cruises in which different analysts used distinct methods for the assessment of nano- and micro-phytoplankton cells (classical taxonomic analysis versus ataxonomic image analysis) suggests that robust patterns of phytoplankton size structure can be obtained by combining data from multiple research programs.

4.2. Persistence of the size-abundance relationship

Heavy departures from linearity in phytoplankton SAS, while virtually absent in oligotrophic, open-ocean environments, have been reported for highly dynamic and productive coastal and shelf waters (Rodríguez et al., 2002; Reul et al., 2006), often during transient blooms in which most of the biomass is contributed by a few species within a small number of size classes. However, most observations of strong non-linearity in phytoplankton SAS have limited temporal and spatial coverage, focusing on specific geographic areas or particular time periods. Surveys with a wide temporal and geographical coverage are required to assess the persistence of the inverse relationship between phytoplankton cell size and abundance. Using a dataset of monthly phytoplankton observations during a 10-yr period in a productive, shelf ecosystem, Huete-Ortega et al. (2010) demonstrated that the inverse relationship between cell size and abundance was persistent throughout the water column and across seasonal and inter-annual time scales. Our analysis extends this persistence over a wide geographical range, as the inverse relationship beween cell size and abundance is found consistently in productive waters of the Benguela upwelling system, the SE Brazil shelf, the Patagonian shelf-break, and the NW Iberia upwelling system. The pervasiveness of the inverse size-abundance relationship reflects a general ecological pattern, whereby population abundance is related to the ratio between resource supply and individual resource requirement, with the latter being largely determined by body size (Brown et al., 2004). This mechanism does not assume energetic equivalence among size classes (Isaac et al., 2012), but derives from the fact that inter-specific variability in the ability to extract resources from the environment (represented in traits such as biomass-normalized maximum nutrient uptake and maximum growth rate) is much smaller (a range of ca. 1 order of magnitude) than the variability in resource requirements (a range of > 6 orders of magnitude in elemental cell quotas) (Edwards et al., 2012, Marañón et al., 2013). A practical implication is that, when dealing with assemblages of phytoplankton species of widely different cell sizes, arguments about ecological dominance should be based on biomass rather than abundance. The fact that the inverse size-abundance relationship holds across widely contrasting environments supports the view that when growth conditions improve most phytoplankton species tend to experience, albeit with different intensity, increases in abundance (Barber and Hiscock, 2006).

4.3. Latitudinal variability in phytoplankton biomass and SAS slope

Combining data from multiple cruises allowed us to characterize the patterns of latitudinal variability in phytoplankton biomass and SAS slope, based on data from 10 to 20 stations for each 10° latitudinal range. As expected, variability in phytoplankton biomass for each band of latitude is much higher in temperate regions than in tropical and subtropical environments, reflecting stronger seasonal changes. The resulting estimates of surface phytoplankton biomass, ranging from mean values of ca. 10 mgC m^{-3} in the subtropical gyres to > 40 mgC m^{-3} in temperate waters, coincide with independent estimates from backscattering measurements during AMT-22 (Fox et al., 2022) and from cell counts obtained with flow cytometry and microscopy during AMT-25 (Brotas et al., 2022). Given the observed values of chlorophyll *a* concentration, these estimates of phytoplankton carbon imply that the C:Chl *a* ratio of surface phytoplankton assemblages in the open ocean can range widely between 100 and 200 in the tropical and subtropical regions and < 50 in temperate latitudes. If we consider also highly productive coastal waters, such as those of NW Iberia, the mean C:Chl *a* ratio can be as low as 30. Hence, as one moves from oligotrophic to eutrophic waters, both phytoplankton carbon biomass and chlorophyll *a* concentration increase, but the latter increases faster. These results highlight the limitations of using chlorophyll *a* concentration as a proxy for phytoplankton biomass even when observations are restricted to surface waters (Graff et al., 2015). The decreased C:Chl *a* in more productive temperate and coastal regions compared to the oligotrophic tropical ocean likely results from the effect of lower incident irradiance and higher nutrient availability, as both conditions lead to enhanced cellular pigment content (Geider, 1987; Halsey and Jones, 2015).

The depth of the nutricline is a proxy of nutrient supply to the euphotic layer, whose latitudinal variability in the Atlantic Ocean has been shown to drive changes in phytoplankton biomass and growth rates (Marañón et al., 2000) as well as in the relative abundance and species richness of diatoms versus coccolithophorids (Cermeño et al., 2008). Our analysis suggests also a relationship between the nutricline depth and the slope of the SAS, with steeper slopes in the subtropical gyres, indicating increased dominance by small cells, associated with greater nutricline depths and a stronger degree of nutrient limitation that results in lower phytoplankton biomass. In temperate regions, increased phytoplankton biomass and shallower nutricline depths are mirrored by less steep SAS slopes, corresponding to enhanced biomass contribution of larger cells. The positive relationship over broad latitudinal scales between nutrient supply and the contribution of large cells in the Atlantic Ocean has been found in simulations with a trait-based model (Acevedo-Trejos et al., 2018) and recently in studies in which phytoplankton cell size and abundance was assessed with imaging flow cytometry (Haëntjens et al., 2022) and with flow cytometry and microscopy (Brotas et al., 2022). However, the degree of covariation

between SAS slope and phytoplankton biomass in open-ocean waters within 50°N–50°S is modest. When the range of total phytoplankton biomass is small (<10-fold), the relationship between SAS slope and phytoplankton standing stocks (represented by total biovolume or carbon biomass) weakens and can even disappear entirely (Moreno-Ostos et al., 2015). This is because similar increases in total phytoplankton biomass or biovolume can result from an increase in the intercept of the SAS, or from the SAS slope becoming less negative (a flattening of the SAS). In the oligotrophic ocean, small cells contribute significantly to the variability in phytoplankton stocks and productivity (Marañón et al., 2001; Huete-Ortega et al., 2011), which can lead to a disconnect between SAS slope and total biovolume and carbon.

4.4. Similarity in SAS slope throughout the euphotic layer

While changes in phytoplankton composition with depth are well documented in stratified ocean regions, both in terms of individual species abundance (Venrick, 1990; Venrick, 1999; Poulton et al., 2017) and dominance by different taxonomic groups (Veldhuis and Kraays, 2004; Mojica et al., 2015; Latasa et al., 2017), consistent patterns in the vertical variability of phytoplankton size structure have been more elusive. Size abundance spectra obtained during stratified conditions in the Sargasso Sea showed a trend towards more negative slopes with increasing depth, indicating an increased biomass contribution by small cells near the base of the euphotic layer (Gin et al., 1999). Similarly, an analysis of > 80 size-fractionated Chl *a* profiles in the north and south Atlantic subtropical gyres revealed an increase in the contribution of the < 2 μm size fraction (picophytoplankton) with depth, from ca. 60% at the surface to ca. 80% at the DCM (Pérez et al., 2006). In contrast, vertical profiles of diagnostic pigment abundance in tropical regions from cruises AMT12-15 indicated the opposite pattern, with the contribution of nano- and microphytoplankton increasing from < 50% at the surface to > 75% at the base of the euphotic layer (Poulton et al., 2006). More recently, relatively invariant contributions of picophytoplankton to total Chl *a* were reported across the euphotic layer in a 30°N to 30°S latitudinal transect in the Atlantic Ocean (Moreno-Ostos et al., 2011). Our analysis of SAS slopes suggests that phytoplankton size structure is largely similar between surface and deep waters across the stratified open ocean, so that the horizontal (geographical) component of variability largely overrides the vertical one. One possible explanation for the lack of significant depth-related differences in size structure is that small cell size provides competitive advantage for the acquisition of both light and nutrients (Raven, 1998; Kiørboe, 2008), but these two resources display opposite vertical gradients, which may counterbalance their effect on the dominance by different size classes. Additional studies with higher vertical resolution will be needed to fully characterize the vertical variability in phytoplankton SAS slopes over large spatial scales in the open ocean.

4.5. Changes in SAS slope across a wide trophic gradient

We have found a basin-scale relationship between increasing resource supply and progressively less steep SAS slopes, reflecting increasing importance of large cells. This pattern confirms earlier results of studies in which size structure was assessed with measurements of size-fractionated Chl *a* (Marañón et al., 2012; Marañón et al., 2015; Poulton et al., 2006) or phytoplankton carbon biomass in a few size classes (Brotas et al., 2022). It must be highlighted that the resource supply index used here includes also a term (the ratio between the depths of the euphotic layer and upper mixed layer) representing light availability. Although in our dataset most of the variability in resource supply was driven by changes in nutrient supply, irradiance has also been shown to be a relevant factor for phytoplankton size structure, explaining the increased contribution of small cells under low-light, high-nutrient conditions in both temperate (Cermeño et al., 2006) and polar environments (Clarke et al., 2008).

Seawater temperature varied widely across the sampled regions but we found that SST explains a negligible amount of the variability in SAS slopes. This result agrees with the findings of Barnes et al. (2011), who found no relationship between SST and the slope of the normalized biomass size spectra in a dataset covering multiple coastal and open-ocean environments. While it is well established that temperature affects the mean population cell size of aquatic protist populations (Atkinson et al., 2003), the variability in phytoplankton size structure observed across the ocean mostly results from changes in the relative abundance of different species, rather than changes in mean intrapopulation cell size (Marañón, 2015, Sommer et al., 2017).

The overall relationship between chlorophyll *a* concentration and both SAS slope and mean community cell size was saturating, which means that there is no indefinite, continuous change towards a dominance by ever larger size classes as ecosystem productivity increases. Rather, similar SAS and mean cell sizes slopes are found in samples with intermediate and high chlorophyll *a* concentration. A similar pattern was found by Barnes et al. (2011), who reported that the slope of the phytoplankton normalized biomass spectrum becomes less steep with increasing primary production (PP) until ca. 400 mgC m^{-2} d^{-1}, while similar slopes are found for sites with PP of 700 and 2800 mgC m^{-2} d^{-1}.

A potential bias in our analysis comes from the fact that the largest phytoplankton species (with a cell volume between 10^6 and 10^7 μm^3), due to their very low abundance (<100 cell L^{-1}), can be missed in conventional (10–50 mL) sampling volumes. We assessed the effect of this underestimation on total phytoplankton biomass and mean cell size, by taking a typical SAS from a coastal, productive site (Ría de Vigo) and adding 4 more size classes (with nominal cell volumes from 1 to 8.4 million μm^3) for which abundance was estimated by applying the observed SAS intercept and slope. The result was an increase in total phytoplankton biomass of 12%, and an increase in the mean ESD from 15 μm to 19 μm. Therefore the pattern observed in Fig. 6b would not change substantially if larger cells (volume > 10^6 μm^3) were considered. It must also be noted that these very large cells, such as the diatom *Coscinodiscus wailesii*, tend to occur in coastal waters only during short periods of time, typically in late winter or early spring, and are very rare during the rest of the year (Tada et al., 2000).

We found a similar size-partitioning of biomass, with a dominance by cells within the 2–20 μm size range (ca. 100–10,000 μm^3 in cell volume), in both moderately and highly eutrophic waters. The biomass dominance of nanophytoplankton in eutrophic ecosystems is in contrast with the results of size-fractionated Chl *a* measurements, which suggests that > 80–90% of all biomass in productive waters is accounted for by the microphytoplankton size class (Marañón et al., 2012). The discrepancy likely results from an overestimation of Chl *a* in the > 20 μm class by size-fractionated filtration methods in phytoplankton-rich waters, resulting from filter clogging and the presence of long chains of cells (Marañón, 2015). The biomass dominance of intermediate-size cells in both meso- and eutrophic systems is linked to the unimodal size scaling of phytoplankton growth and the fact that maximum growth rates decrease with increasing cell size for phytoplankton cells larger > 10 μm (Marañón et al., 2013; Hillebrand et al., 2022), which together with increasing sinking losses may counterbalance the benefits of large cell size as a refuge from predation (Pancic and Kiørboe, 2018). Our results thus support the results of recent observational and modelling studies that highlight the importance of intermediate-size cells in nutrient-rich, productive environments (Bolaños et al., 2020; Juranek et al., 2020; Montes-Pérez et al., 2020; Negrete-García et al., 2022).

Finally, the nutrient-driven biogeographic pattern in SAS slopes has implications for the prediction of ecosystem responses to global change across the ocean. In regions such as the subtropical gyres, where increased oligotrophication may lead to a decrease in phytoplankton standing stocks, enhanced contributions of small cells may be expected. In contrast, if climate change leads to higher primary production, as seems to be the case in some polar regions (Lewis et al., 2020), an increased dominance by larger cells may take place. In some coastal

regions exposed to growing inputs of anthropogenic nutrients (Maúre et al., 2021), an increased contribution of larger cells can also be anticipated. Because of the linkage between phytoplankton size structure and the fate of primary production, these changes may reinforce the geographical variability in the potential of different marine regions to sustain the downward export of organic carbon.

5. Conclusions

A large, multi-cruise dataset demonstrates that the inverse relationship between phytoplankton cell size and abundance is pervasive even in nutrient-rich, productive waters. Our analysis reveals a resource-driven, biogeographic pattern in phytoplankton size structure that is common to both surface and deep waters within the euphotic layer over large spatial scales in the Atlantic Ocean. We have also characterized the latitudinal variability in phytoplankton biomass and size structure, which reflects changes in nutrient supply as represented by the nutricline depth. The overall non-linear relationship between trophic status and SAS slope underscores the pivotal role of intermediate-size cells for primary productivity and energy transfer in the most productive pelagic ecosystems. This study illustrates how combining multiple datasets of phytoplankton abundance can contribute to a size-based characterization of pelagic ecosystems. Emergent automated and semi-automated optical methods (Juranek et al., 2020; Haëntjens et al., 2022) will be key to improve the spatial and temporal resolution of observations of phytoplanton size-abundance spectra in the ocean.

Data availability statement

The phytoplankton size-abundance data from the Ría de Vigo annual surveys are available at https://doi.org/10.5281/zenodo.8138107. Phytoplankton data from the RADIALES program are available at https://doi.org/10.1594/PANGAEA.777384. Data from the ACEx cruise are available at https://doi.org/10.1594/PANGAEA.855752. Data from the AMT and the Benguela cruises are available at the British Oceanographic Data Centre (https://www.bodc.ac.uk/). Data from other programs and surveys listed in Table S1 can be obtained from the authors upon request.

Declaration of Competing Interest

The authors declare that they have no known competing financial interests or personal relationships that could have appeared to influence the work reported in this paper.

Acknowledgements

We thank all the researchers who contributed to the collection and analysis of samples and data as well as the captain and crew of all oceanographic vessels involved in the different surveys and programs. This research was supported by the European Union through H2020 TRIATLAS project 'Tropical and South Atlantic climate-based marine ecosystem predictions for sustainable management' (Grant agreement No. 817578) and by the Spanish Ministry of Science and Innovation through research grants CTM2008-03699, CSD2008-00077, CTM2004-05174-C02 and REN2000-1248. The Atlantic Meridional Transect is funded by the UK Natural Environment Research Council through its National Capability Long-term Single Centre Science Programme, Climate Linked Atlantic Sector Science (grant number NE/R015953/1). This study contributes to the international IMBeR project and is contribution number 388 of the AMT programme. The RADIALES program is supported by Instituto Español de Oceanografía (Spain) and additional funds from Xunta de Galicia (Spain) through grant IN607A2022-05. The ACEx/SIMTECO cruise was supported by the Brazilian National Council for Scientific and Technological Development (CNPq, grant 558108/2009-1) and the Funding Authority for Studies and Projects (FINEP). The PATEX cruise was supported by the Brazilian National Council for Scientific and Technological Development (CNPq, grant 520189/ 2006-0). The Abraços 2 cruise was funded by the the French oceanographic fleet.

Appendix A. Supplementary data

Supplementary data to this article can be found online at https://doi.org/10.1016/j.pocean.2023.103104.

References

Acevedo-trejos, E., Marañón, E., Acevedo-trejos, E., Merico, A., Marañón, E., Merico, A., 2018. Phytoplankton size diversity and ecosystem function relationships across oceanic regions. Proc. Royal Soc. B 285. https://doi.org/10.1098/rspb.2018.0621.

Armstrong, R.A., 1994. Grazing limitation and nutrient limitation in marine ecosystems: Steady state solutions of an ecosystem model with multiple food chains. Limnol. Oceanogr. 39, 597–608 https://doi.org/https://doi.org/10.4319/lo.1994.39.3.0597.

Atkinson, D., Ciotti., B.J., Montagnes, D.S.J., 2003. Protists decrease in size linearly with temperature: ca. 2.5% $^{\circ}C^{-1}$. Proc. R. Soc. B 270, 2605–2611 https://doi.org/10.1098/rspb.2003.2538.

Barber, R.T., Hiscock, M.R., 2006. A rising tide lifts all phytoplankton: Growth response of other phytoplankton taxa in diatom-dominated blooms. Global Biogeochem. Cycles 20 https://doi.org/10.1029/2006GB002726.

Barnes, C., Irigoien, X., De Oliveira, J.A.A., Maxwell, D., Jennings, S., 2011. Predicting marine phytoplankton community size structure from empirical relationships with remotely sensed variables. J. Plankton Res. 33, 13–24. https://doi.org/10.1093/plankt/fbq088.

Barton, A.D., Pershing, A.J., Litchman, E., Record, N.R., Edwards, K.F., Finkel, Z.V., Kiørboe, T., Ward, B.A., 2013. The biogeography of marine plankton traits. Ecol. Lett. 16, 522–534. https://doi.org/10.1111/ele.12063.

Bolaños, L.M., Karp-Boss, L., Choi, C.J., Worden, A.Z., Graff, J.R., Haëntjens, N., Chase, A.P., della Penna, A., Gaube, P., Morison, F., Menden-Deuer, S., Westberry, T.K., O'Malley, R.T., Boss, E., Behrenfeld, M.J., Giovannoni, S.J., 2020. Small phytoplankton dominate western North Atlantic biomass. ISME J. 14, 1663–1674. https://doi.org/10.1038/s41396-020-0636-0.

Brotas, V., Tarran, G.A., Veloso, V., Brewin, R.J.W., Woodward, E.M.S., Airs, R., Beltran, C., Ferreira, A., Groom, S.B., 2022. Complementary approaches to assess phytoplankton groups and size classes on a long transect in the Atlantic ocean. Front. Mar. Sci. 8, 1–17. https://doi.org/10.3389/fmars.2021.682621.

Brown, J.H., Gillooly, J.F., Allen, A.P., Savage, V.M., West, G.B., 2004. Toward a metabolic theory of ecology. Ecology 85, 1771–1789. https://doi.org/10.1890/03-9000.

Buitenhuis, E.T., Li, W.K.W., Vaulot, D., Lomas, M.W., Landry, M.R., Partensky, F., Karl, D.M., Ulloa, O., Campbell, L., Jacquet, S., Lantoine, F., Chavez, F., Macias, D., Gosselin, M., McManus, G.B., 2012. Picophytoplankton biomass distribution in the global ocean. Earth Syst. Sci. Data Discuss. 5, 221–242. https://doi.org/10.5194/essdd-5-221-2012.

Cavender-Bares, K.K., Karl, D.M., Chisholm, S.W., 2001. Nutrient gradients in the western North Atlantic Ocean: Relationship to microbial community structure and comparison to patterns in the Pacific Ocean. Deep Sea Res. Part I Oceanogr. Res. Pap. 48, 2373–2395. https://doi.org/10.1016/S0967-0637(01)00027-9.

Cermeño, P., Marañón, E., Pérez, V., Serret, P., Fernández, E., Castro, C.G., 2006. Phytoplankton size structure and primary production in a highly dynamic coastal ecosystem (Ría de Vigo, NW-Spain): Seasonal and short-time scale variability. Estuar. Coast. Shelf Sci. 67, 251–266. https://doi.org/10.1016/j.ecss.2005.11.027.

Cermeño, P., Dutkiewicz, S., Harris, R.P., Follows, M., Schofield, O., Falkowski, P.G., 2008. The role of nutricline depth in regulating the ocean carbon cycle. Proc. Natl. Acad. Sci. U S A 105, 20344–20349. https://doi.org/10.1073/pnas.0811302106.

Chisholm, S.W., 1992. Phytoplankton Size. In: Falkowski, P.G., Woodhead, A.D., Vivirito, K. (eds) Primary Productivity and Biogeochemical Cycles in the Sea. Environmental Science Research, vol 43. Springer, Boston, MA. https://doi.org/10.1007/978-1-4899-0762-2_12.

Clarke, A., Meredith, M.P., Wallace, M.I., Brandon, M.A., Thomas, D.N., 2008. Seasonal and interannual variability in temperature, chlorophyll and macronutrients in northern Marguerite Bay, Antarctica. Deep Sea Res. II Top. Stud. Oceanogr. 55, 1988–2006. https://doi.org/10.1016/j.dsr2.2008.04.035.

Culverhouse, P., Williams, R., Reguera, B., Herry, V., González-Gil, S., 2003. Do experts make mistakes? A comparison of human and machine identification of dinoflagellates. Mar. Ecol. Prog. Ser. 247, 17–25. https://doi.org/10.3354/meps247017.

Edwards, K.F., Thomas, M.K., Klausmeier, C.A., Litchman, E., 2012. Allometric scaling and taxonomic variation in nutrient utilization traits and maximum growth rate of phytoplankton. Limnol. Oceanogr. 57, 554–566. https://doi.org/10.4319/lo.2012.57.2.0554.

Fox, J., Kramer, S.J., Graff, J.R., Behrenfeld, M.J., Boss, E., Tilstone, G., Halsey, K.H., 2022. An absorption-based approach to improved estimates of phytoplankton biomass and net primary production. Limnol. Oceanogr. Lett. 7, 419–426. https://doi.org/10.1002/lol2.10275.

Geider, R.J., 1987. Light and temperature dependence of the carbon to chlorophyll a ratio in microalgae and cyanobacteria: implications for physiology and growth of phytoplankton. New Phytologist 106, 1–34.
Gin, K.Y.H., Chisholm, S.W., Olson, R.J., 1999. Seasonal and depth variation in microbial size spectra at the Bermuda Atlantic time series station. Deep Sea Res. Part I Oceanogr. Res. Pap. 46, 1221–1245. https://doi.org/10.1016/S0967-0637(99)00004-7.
Gonçalves-Araujo, R., de Souza, M.S., Mendes, C.R.B., Tavano, V.M., Pollery, R.C., Garcia, C.A.E., 2012. Brazil-Malvinas confluence: Effects of environmental variability on phytoplankton community structure. J. Plankton Res. 34, 399–415. https://doi.org/10.1093/plankt/fbs013.
Gonçalves-Araujo, R., de Souza, M.S., Tavano, V.M., Mendes, C.R., de Souza, R.B., Schultz, C., Pollery, R.C., 2018. Phyto- and protozooplankton assemblages and hydrographic variability during an early winter survey in the Southern Brazilian Continental Shelf. J. Mar. Syst. 184, 36–49. https://doi.org/10.1016/j.jmarsys.2018.04.005.
Graff, J.R., Westberry, T.K., Milligan, A.J., Brown, M.B., Dall'Olmo, G., van Dongen-Vogels, V., Reifel, K.M., Behrenfeld, M.J., 2015. Analytical phytoplankton carbon measurements spanning diverse ecosystems. Deep Sea Res. I Oceanogr. Res. Pap. 102, 16–25. https://doi.org/10.1016/j.dsr.2015.04.006.
Haëntjens, N., Boss, E.S., Graff, J.R., Chase, A.P., Karp-Boss, L., 2022. Phytoplankton size distributions in the western North Atlantic and their seasonal variability. Limnol. Oceanogr. 67, 1865–1878. https://doi.org/10.1002/lno.12172.
Halsey, K.H., Jones, B.M., 2015. Phytoplankton strategies for photosynthetic energy allocation. Ann. Rev Mar. Sci. 7, 265–297. https://doi.org/10.1146/annurev-marine-010814-015813.
Harrison, P.J., Zingone, A., Mickelson, M.J., Lehtinen, S., Ramaiah, N., Kraberg, A.C., Sun, J., McQuatters-Gollop, A., Jakobsen, H.H., 2015. Cell volumes of marine phytoplankton from globally distributed coastal data sets. Est. Coast. Shelf Sci. 162, 130–142. https://doi.org/10.1016/j.ecss.2015.05.026.
Hillebrand, H., Acevedo-Trejos, E., Moorthi, S.D., Ryabov, A., Striebel, M., Thomas, P.K., Schneider, M.L., 2022. Cell size as driver and sentinel of phytoplankton community structure and functioning. Funct. Ecol. 36, 276–293. https://doi.org/10.1111/1365-2435.13986.
Huete-Ortega, M., Marañón, E., Varela, M., Bode, A., 2010. General patterns in the size scaling of phytoplankton abundance in coastal waters during a 10-year time series. J. Plankton Res. 32, 1–14. https://doi.org/10.1093/plankt/fbp104.
Huete-Ortega, M., Calvo-Díaz, A., Graña, R., Mouriño-Carballido, B., Marañón, E., 2011. Effect of environmental forcing on the biomass, production and growth rate of size-fractionated phytoplankton in the central Atlantic Ocean. J. Mar. Syst. 88, 203–213. https://doi.org/10.1016/j.jmarsys.2011.04.007.
Huete-Ortega, M., Cermeño, P., Calvo-Díaz, A., Marañón, E., 2012. Isometric size-scaling of metabolic rate and the size abundance distribution of phytoplankton. Proc. Royal Soc. B 279, 1815–1823. https://doi.org/10.1098/rspb.2011.2257.
Isaac, N.J.B., Storch, D., Carbone, C., 2012. The paradox of energy equivalence. Glob. Ecol. Biogeo. 22, 1–5. https://doi.org/10.1111/j.1466-8238.2012.00782.x.
Juranek, L.W., White, A.E., Dugenne, M., Henderikx Freitas, F., Dutkiewicz, S., Ribalet, F., Ferrón, S., Armbrust, E.V., Karl, D.M., 2020. The Importance of the Phytoplankton "Middle Class" to Ocean Net Community Production. Global Biogeochem. Cycles 34. https://doi.org/10.1029/2020GB006702.
Karlson, B., Andreasson, A., Johansen, M., Karlberg, M., Loo, A., Skjevik, A-T., 2020. Nordic Microalgae. World-wide electronic publication, http://nordicmicroalgae.org.
Kiørboe, T., 2008. A mechanistic approach to plankton ecology. Princeton University Press.
Latasa, M., Cabello, A.M., Morán, X.A.G., Massana, R., Scharek, R., 2017. Distribution of phytoplankton groups within the deep chlorophyll maximum. Limnol. Oceanogr. 62, 665–685. https://doi.org/10.1002/lno.10452.
Lewis, K.M., Van Dijken, G.L., Arrigo, K.R., 2020. Changes in phytoplankton concentration now drive increased Arctic Ocean primary production. Science 369, 198–202 https://doi.org//10.1126/science.aay8380.
Marañón, E., 2015. Cell Size as a Key Determinant of Phytoplankton Metabolism and Community Structure. Ann. Rev. Mar. Sci. 7, 241–264. https://doi.org/10.1146/annurev-marine-010814-015955.
Marañón, E., Holligan, P.M., Varela, M., Mourin, B., Bale, A.J., Mouriño, B., Bale, A.J., 2000. Basin-scale variability of phytoplankton biomass, production and growth in the Atlantic Ocean. Deep Sea Res. I Oceanogr. Res. Pap. 47, 825–857.
Marañón, E., Holligan, P.M., Barciela, R., González, N., Mouriño, B., Pazó, M.J., Varela, M., 2001. Patterns of phytoplankton size structure and productivity in contrasting open-ocean environments. Mar. Ecol. Prog. Ser. 216, 43–56. https://doi.org/10.3354/meps216043.
Marañón, E., Cermeño, P., Fernández, E., Rodríguez, J., Zabala, L., 2004. Significance and mechanisms of photosynthetic production of dissolved organic carbon in a coastal eutrophic ecosystem. Limnol. Oceanogr. 49, 1652–1666. https://doi.org/10.4319/lo.2004.49.5.1652.
Marañón, E., Cermeño, P., Rodríguez, J., Zubkov, M.V., Harris, R.P., 2007. Scaling of phytoplankton photosynthesis and cell size in the ocean. Limnol. Oceanogr. 52, 2190–2198. https://doi.org/10.4319/lo.2007.52.5.2190.
Marañón, E., Cermeño, P., Latasa, M., Tadonléké, R.D., 2012. Temperature, resources, and phytoplankton size structure in the ocean. Limnol. Oceanogr. 57, 1266–1278. https://doi.org/10.4319/lo.2012.57.5.1266.
Marañón, E., Cermeño, P., López-Sandoval, D.C., Rodríguez-Ramos, T., Sobrino, C., Huete-Ortega, M., Blanco, J.M., Rodríguez, J., 2013. Unimodal size scaling of phytoplankton growth and the size dependence of nutrient uptake and use. Ecol. Lett. 16, 371–379 https://doi.org/10.1111/ele.12052.
Marañón, E., Cermeño, P., Huete-Ortega, M., López-Sandoval, D.C., Mouriño-Carballido, B., Rodríguez-Ramos, T., Marañón, E., Cermeño, P., Huete-Ortega, M., López-Sandoval, D.C., Mouriño-Carballido, B., Rodríguez-Ramos, T., 2014. Resource supply overrides temperature as a controlling factor of marine phytoplankton growth. PLoS One 9, 20–23. https://doi.org/10.1371/journal.pone.0099312.
Marañón, E., Cermeño, P., Latasa, M., Tadonléké, R.D., 2015. Resource supply alone explains the variability of marine phytoplankton size structure. Limnol. Oceanogr. 60, 1848–1854. https://doi.org/10.1002/lno.10138.
Maúre, E.d.R., Terauchi, G., Ishizaka, J., Clinton, N., DeWitt, M., 2021. Globally consistent assessment of coastal eutrophication. Nat. Commun. 12, 6142. https://doi.org/10.1038/s41467-021-26391-9.
Mojica, K.D.A., van de Poll, W.H., Kehoe, M., Huisman, J., Timmermans, K.R., Buma, A.G.J., van der Woerd, H.J., Hahn-Woernle, L., Dijkstra, H.A., Brussaard, C.P.D., 2015. Phytoplankton community structure in relation to vertical stratification along a north-south gradient in the Northeast Atlantic Ocean. Limnol. Oceanogr. 60, 1498–1521. https://doi.org/10.1002/lno.10113.
Montes-Pérez, J.J., Moreno-Ostos, E., Marañón, E., Blanco, J.M., Rodríguez, V., Rodríguez, J., 2020. Intermediate-size cell dominance in the phytoplankton community of an eutrophic, estuarine ecosystem (Guadalhorce River, Southern Spain). Hydrobiologia 847, 2241–2254. https://doi.org/10.1007/s10750-020-04251-9.
Moreno-Ostos, E., Fernández, A., Huete-Ortega, M., Mouriño-Carballido, B., Calvo-Díaz, A., Morán, X.A.G., Marañón, E., 2011. Size-fractionated phytoplankton biomass and production in the tropical Atlantic. Sci. Mar. 75, 379–389. https://doi.org/10.3989/scimar.2011.75n2379.
Moreno-Ostos, E., Blanco, J.M., Agustí, S., Lubián, L.M., Rodríguez, V., Palomino, R.L., Llabrés, M., Rodríguez, J., 2015. Phytoplankton biovolume is independent from the slope of the size spectrum in the oligotrophic Atlantic Ocean. J. Mar. Syst. 152, 42–50. https://doi.org/10.1016/j.jmarsys.2015.07.008.
Negrete-García, G., Luo, J.Y., Long, M.C., Lindsay, K., Levy, M., Barton, A.D., 2022. Plankton energy flows using a global size-structured and trait-based model. Prog. Oceanogr. 209, 102898 https://doi.org/10.1016/j.pocean.2022.102898.
Olenina, I., Hajdu, S., Edler, L., Andersson, A., Wasmund, N., Busch, S., Göbel, J., Gromisz, S., Huseby, S., Huttunen, M., Jaanus, A., Kokkonen, P., Ledaine, I., Niemkiewicz, E., 2006. Biovolumes and Size-Classes of Phytoplankton in the Baltic Sea. Helsinki Commission Baltic Sea Environment Proceedings.
Orízar, I.D.S., Lewandowska, A.M., 2022. Intraspecific Trait Variability of a Diatom and a Dinoflagellate Along a Salinity Gradient. Front. Mar. Sci. 9 https://doi.org/10.3389/fmars.2022.880309.
Pančić, M., Kiørboe, T., 2018. Phytoplankton defence mechanisms: traits and trade-offs. Biol. Rev. 93, 1269–1303. https://doi.org/10.1111/brv.12395.
Pérez, V., Fernández, E., Marañón, E., Morán, X.A.G., Zubkov, M.V., 2006. Vertical distribution of phytoplankton biomass, production and growth in the Atlantic subtropical gyres. Deep Sea Res. I Oceanogr. Res. Pap. 53, 1616–1634. https://doi.org/10.1016/j.dsr.2006.07.008.
Peter, K.H., Sommer, U., 2013. Phytoplankton Cell Size Reduction in Response to Warming Mediated by Nutrient Limitation. PLoS One 8, 1–6. https://doi.org/10.1371/journal.pone.0071528.
Poulin, F.J., Franks, P.J.S., 2010. Size-structured planktonic ecosystems: constraints, controls and assembly instructions. J. Plankton Res. 32, 1121–1130. https://doi.org/10.1093/plankt/fbp145.
Poulton, A.J., Holligan, P.M., Hickman, A., Kim, Y.-N., Adey, T.R., Stinchcombe, M.C., Holeton, C., Root, S., Woodward, E.M.S., 2006. Phytoplankton carbon fixation, chlorophyll-biomass and diagnostic pigments in the Atlantic Ocean. Deep Sea Res. Part II Top. Stud. Oceanogr. 53, 1593–1610. https://doi.org/10.1016/j.dsr2.2006.05.007.
Poulton, A.J., Holligan, P.M., Charalampopoulou, A., Adey, T.R., 2017. Coccolithophore ecology in the tropical and subtropical Atlantic Ocean: New perspectives from the Atlantic meridional transect (AMT) programme. Prog. Oceanogr. 158, 150–170. https://doi.org/10.1016/j.pocean.2017.01.003.
Raimbault, P., Rodier, M., Taupier-Letage, I., 1988. Size fraction of phytoplankton in the Ligurian Sea and the Algeria Basin (Mediterranean Sea): size distribution versus total concentration. Mar. Microb. Food Webs 3, 1–7.
Raven, J.A., 1998. The twelfth Tansley Lecture. Small is beautiful: the picophytoplankton. Funct. Ecol. 12, 503–513. https://doi.org/10.1046/j.1365-2435.1998.00233.x.
Reul, A., Rodríguez, V., Jiménez-Gómez, F., Blanco, J.M., Bautista, B., Sarhan, T., Guerrero, F., Ruíz, J., García-Lafuente, J., 2005. Variability in the spatio-temporal distribution and size-structure of phytoplankton across an upwelling area in the NW-Alboran Sea, (W-Mediterranean). Cont. Shelf Res. 25, 589–608. https://doi.org/10.1016/j.csr.2004.09.016.
Reul, A., Rodríguez, J., Blanco, J.M., Rees, A., Burkill, P.H., 2006. Control of microplankton size structure in contrasting water columns of the Celtic Sea. J. Plankton Res. 28, 449–457. https://doi.org/10.1093/plankt/fbi120.
Rodríguez, J., Jiménez-Gómez, F., Blanco, J.M., Figueroa, F.L., 2002. Physical gradients and spatial variability of the size structure and composition of phytoplankton in the Gerlache Strait (Antarctica). Deep Sea Res. II Top. Stud. Oceanogr. 49, 693–706. https://doi.org/10.1016/S0967-0645(01)00119-9.
Rodríguez, J., Blanco, J.M., Jiménez-Gómez, F., Echevarría, F., Gil, J., Rodríguez, V., Ruiz, J., Bautista, B., Guerrero, F., 1998. Patterns in the size structure of the phytoplankton community in the deep fluorescence maximum of the Alboran Sea. Deep Sea Res. Part I Oceanogr. Res. Pap. 45, 1577–1593. https://doi.org/10.1016/S0967-0637(98)00030-2.
Sal, S., López-Urrutia, Á., Irigoien, X., Harbour, D.S., Harris, R.P., 2013. Marine microplankton diversity database. Ecology 94, 1658. https://doi.org/10.1890/13-0236.1.

Sommer, U., Peter, K.H., Genitsaris, S., Moustaka-Gouni, M., 2017. Do marine phytoplankton follow Bergmann's rule *sensu lato*? Biological Reviews 92, 1011–1026. https://doi.org/10.1111/brv.12266.

Tada, K., Pithakpol, S., Ichimi, K., Montani, S., 2000. Carbon, nitrogen, phosphorus, and chlorophyll *a* content of the large diatom, *Coscinodiscus wailesii* and its abundance in the Seto Inland Sea. Japan. Fish. Sci. 66, 509–514. https://doi.org/10.1046/j.1444-2906.2000.00080.x.

Veldhuis, M.J.W., Kraay, G.W., 2004. Phytoplankton in the subtropical Atlantic Ocean: Towards a better assessment of biomass and composition. Deep Sea Res. I Oceanogr. Res. Pap. 51, 507–530. https://doi.org/10.1016/j.dsr.2003.12.002.

Venrick, E.L., 1990. Phytoplankton in an Oligotrophic Ocean: Species Structure and Interannual Variability. Ecology 71, 1547–1563. https://doi.org/10.2307/1938291.

Venrick, E.L., 1999. Phytoplankton species structure in the central North Pacific 1973–1996: variability and persistence. J. Plankton Res. 21, 1029–1042. https://doi.org/10.1093/plankt/21.6.1029.

Ward, B.A., Dutkiewicz, S., Follows, M.J., 2014. Modelling spatial and temporal patterns in size-structured marine plankton communities: Top-down and bottom-up controls. J. Plankton Res. 36, 31–47. https://doi.org/10.1093/plankt/fbt097.

White, E.P., Ernest, S.K.M., Kerkhoff, A.J., Enquist, B.J., 2007. Relationships between body size and abundance in ecology. Trends Ecol. Evol. 22, 323–330 https://doi.org/10.1016/j.tree.2007.03.007.

Zubkov, M.V., Sleigh, M.A., 2000. Assaying picoplankton distribution by flow cytometry of underway samples collected along a meridional transect across the Atlantic Ocean. Aquat. Microb. Ecol. 21, 13–20 https://doi.org/doi:10.3354/ame021013.

Zubkov, M.V., Sleigh, M.A., Tarran, G.A., Burkill, P.H., Leakey, R.J.G., 1998. Picoplanktonic community structure on an Atlantic transect from 50°N to 50°S. Deep Sea Res. Part I Oceanogr. Res. Pap. 45, 1339–1355. https://doi.org/10.1016/S0967-0637(98)00015-6.